Journal of
Synchrotron
Radiation

ISSN 0909-0495

Received 10 March 2010
Accepted 12 October 2010

Investigations of mechanical vibrations for beamlines at the Canadian Light Source

J. W. Li,[a,b,c] E. Matias,[a] N. Chen,[a] C.-Y. Kim,[a] J. Wang,[a] J. Gorin,[a] F. He,[a] P. Thorpe,[a] Y. Lu,[a] W. F. Chen,[a] P. Grochulski,[a] X. B. Chen[b,c] and W. J. Zhang[b,c]*

[a]Canadian Light Source Inc., 101 Perimeter Road, Saskatoon, Saskatchewan, Canada S7N 0X4, [b]Department of Mechanical Engineering, University of Saskatchewan, 57 Campus Drive, Saskatoon, Canada S7N 5A9, and [c]Division of Biomedical Engineering, University of Saskatchewan, 57 Campus Drive, Saskatoon, Canada S7N 5A9. E-mail: chris.zhang@usask.ca

Vibration is often a problem causing poor quality of photon beams at synchrotron radiation facilities, since beamlines are quite sensitive to vibrations. Therefore, vibration analysis and control at synchrotron radiation facilities is crucial. This paper presents investigations on mechanical vibrations at four beamlines and endstations at the Canadian Light Source, *i.e.* the Canadian Macromolecular Crystallography Facility 08ID-1 beamline, the Hard X-ray MicroAnalysis 06ID-1 beamline, the Resonant Elastic and Inelastic Soft X-ray Scattering 10ID-2 beamline, and the Scanning Transmission X-ray Microscope endstation at the Spectromicroscopy 10ID-1 beamline. This study identifies vibration sources and investigates the influence of mechanical vibrations on beamline performance. The results show that vibrations caused by movable mechanical equipment significantly affect the data acquired from beamlines.

Keywords: vibration; instrumentation; Canadian Light Source.

1. Introduction

In recent decades, synchrotron radiation has developed into a valuable scientific tool for scientists around the world (Terzano *et al.*, 2010; Yates & Hallin, 2002; Michaelian *et al.*, 2008). At synchrotron radiation facilities, the vibration of the electron and/or photon beam, especially in the vertical direction, enlarges its size and changes its intensity. This degrades the performance of the beamline. For instance, it is reported that the amplitude of floor vibrations at KEK's accelerator test facility ATF2 project is approximately 50 μm, which is even larger than the vertical beam spot size expected at ATF2 (Masuzawa *et al.*, 2006). In another report related to synchrotron radiation lithography, the quality of micro-structures fabricated by the lithography beamline is greatly affected when the amplitude of the vibration is larger than a quarter of the minimum feature size (Fukuda *et al.*, 1996).

Many other factors that are responsible for vibrations at synchrotron radiation facilities have been reported in the literature, such as traffic (Wang *et al.*, 2008*a*), human activities (Masuzawa *et al.*, 2006), strong wind and/or ocean waves (Masuzawa *et al.*, 2006), water pipes and moving mechanical components. Thus, careful investigations of vibrations at synchrotron radiation facilities are crucial, especially if the photon beam size is within a few micrometers. It is believed that the vibration issue should be addressed before any sophisticated control system can be designed to improve the stability of the photon beam (Tanaka *et al.*, 2002).

Studies of vibrations have been conducted at synchrotron radiation facilities worldwide. At the SPring-8 storage ring, studies have shown that electron beam orbit fluctuations can be caused by the cooling water (Matsui *et al.*, 2003) and magnet vibrations (Tsumaki & Kumagai, 2001). At the Shanghai Synchrotron Radiation Facility, vibrations caused by the floor, girders, vacuum chamber, magnet, quadrupoles and traffic have been investigated (Wang *et al.*, 2008*a*,*b*; Ouyang *et al.*, 2006; Yin *et al.*, 2007). At the Taiwan Light Source, Liu *et al.* (2007) identified vibration sources in the water and piping systems and studied how vibrations were propagated through the facility. At the National Laboratory for High Energy Physics (KEK) Photon Factory, Huke (1987) studied the correlation between the movement of the building and the vibration of the beam orbit. At KEK's Accelerator Test Facility (ATF), Masuzawa *et al.* (2006) believed that floor vibrations above 50 Hz are caused by human activities. Other vibration studies at synchrotron radiation facilities were reported by Nakazato *et al.* (2002), Doose & Sharma (2002), Wang *et al.* (2002), Aleshaev *et al.* (2001), Preissner & Shu (2006) and Wang *et al.* (2006).

To minimize vibration propagation, the facility floor at the Canadian Light Source (CLS) was designed as follows (Benmerrouche & Hodges, 2010). A reinforced concrete grade beam of depth 600 mm forms the perimeter of the building foundation. The grade beam is supported by drilled and cast-in-place concrete piles at column locations. The experimental hall has a 350 mm-thick reinforced concrete floor, supported

on piles spaced at approximately 4 m in each direction. The experimental hall floor slab is supported on piles, with a void between it and the underlying soil. The floor of the main experimental hall is divided into sections to reduce the transmission of vibrations between high-traffic areas and sensitive-beamline areas. The annular section of floor under the booster ring area is separate and mechanically isolated from the storage ring and experimental area floor, the building superstructure and the service area inside the main storage ring and the new mechanical basement. The shielding over the storage ring rests on the experimental area floor and its own piles. The floor of the north-east building addition is divided into two sections. The foundations will be a continuation of the isolated floor slab to accommodate the beamline components and hutches as well as a separate slab supporting the laboratory and office space.

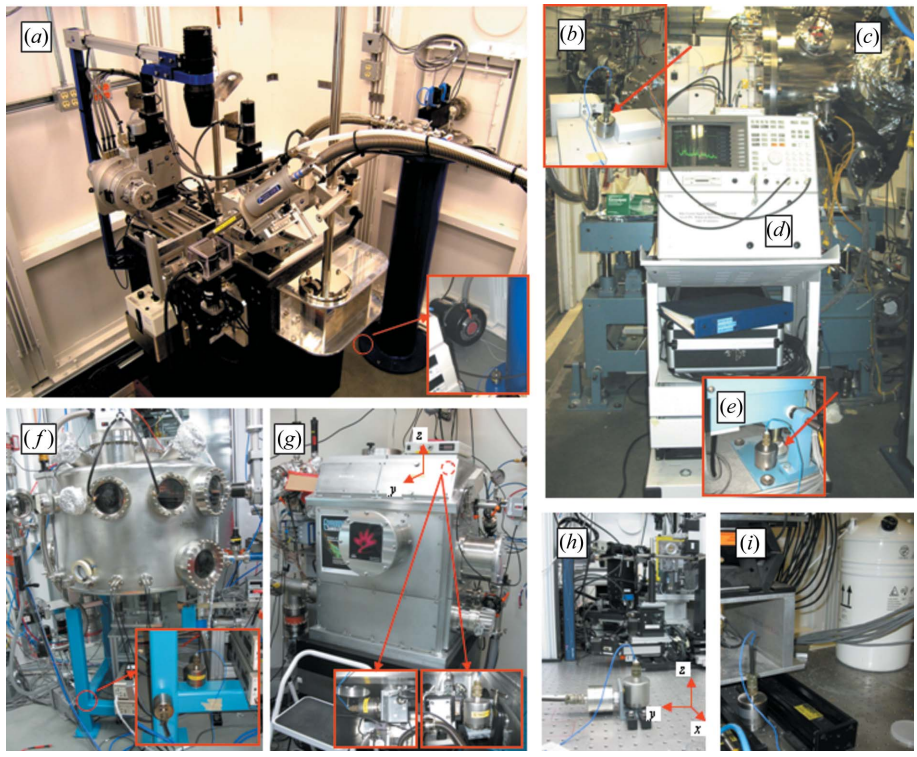

Figure 1
Set-up of accelerometers at various beamlines.

Although the CLS floor was carefully designed, we found that beamline developments still necessitate carrying out vibration studies. In this study we investigated vibrations in the experimental and optics hutches at four beamlines and endstations at the CLS: the Canadian Macromolecular Crystallography Facility (CMCF) 08ID-1 beamline, the Hard X-ray MicroAnalysis (HXMA) 06ID-1 beamline, the Resonant Elastic and Inelastic Soft X-ray Scattering (REIXS) 10ID-2 beamline and the Scanning Transmission X-ray Microscope (STXM) endstation at the Spectromicroscopy (SM) 10ID-1 beamline. This work identified key vibration sources and investigated the influence of mechanical vibrations on beamline performance.

2. Identification of vibration sources

2.1. Instrumentation

The Canadian Light Source Vibration Data Acquisition system was used to measure vibration in the CLS facility (Fig. 1*d*) (Paulsen, 2006). It includes a Vector Signal Analyzer (VSA) (Model: Hp Agilent 89410A; manufacturer: HP) and accelerometers (Model: 393B31; manufacturer: PCB PIEZOTRONICS). Accelerometers produce a voltage proportional to the acceleration of their connected object. The VSA converts the output voltage of the accelerometers into a voltage power spectral density (S_v). Acceleration power spectral density [S_a; units: $(\mathrm{m\ s^{-2}})^2\ \mathrm{Hz^{-1}}$] is obtained from S_v by the following equation (Paulsen, 2006),

$$S_a = S_v/a^2, \tag{1}$$

where a is the sensitivity of the accelerometers. The displacement power spectral density (PSD) (S_d; units: $\mu\mathrm{m^2\ Hz^{-1}}$) is calculated using S_a by the following equation (Paulsen, 2006),

$$S_d = \frac{S_a \times 10^{12}}{(2\pi f)^4}. \tag{2}$$

The root-mean-square (RMS) displacement over a given frequency band (f_1, f_2) can be calculated using the following equation (Paulsen, 2006),

$$Z = \left[\int_{f_1}^{f_2} S_d(f)\,\mathrm{d}f\right]^{1/2}. \tag{3}$$

The sensitivity of the accelerometer $a = 1.02\ \mathrm{V\ (m\ s^{-2})^{-1}}$. The frequency range of the measurement is 1 Hz to 300 Hz. The frequency resolution of the accelerometer is better than 0.1 Hz. In this study we used two indexes for vibration evaluation, *i.e.* the displacement PSD and the RMS displacement. The displacement PSD shows the strength of the displacement variation as a function of frequency. The RMS displacement represents the amplitude of displacement variations within a specific frequency range.

Accelerometers were mounted at various beamlines, as shown in Fig. 1.

2.2. Vibration sources

2.2.1. Fan coil unit. The fan coil unit, as shown in Fig. 2(*a*), is hung on the ceiling in the CMCF 08ID-1 experimental hutch (SOE). The accelerometer is mounted on the blue steel base which is rigidly fixed on the floor, as shown in Fig. 1(*a*). Fig. 3

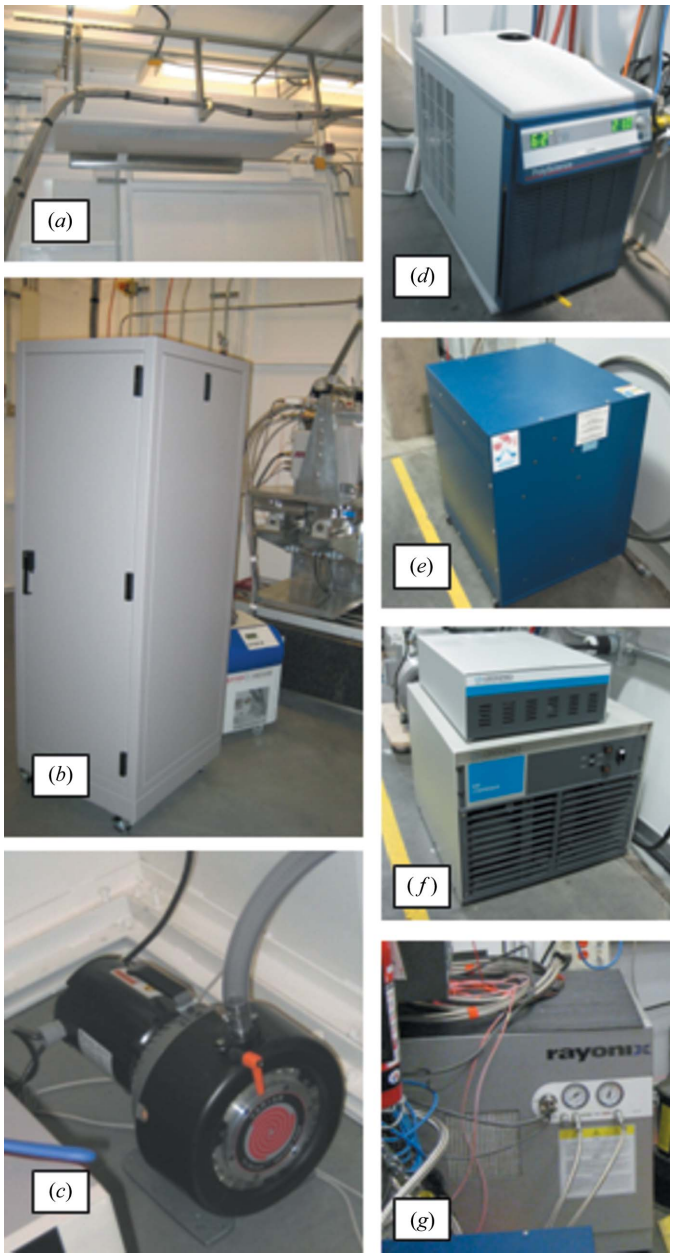

Figure 2
Identified vibration sources.

shows that the induced vibrations of the fan coil unit have frequencies of 25.5 Hz (RMS displacement: 2.0×10^{-4} µm), 26.5 Hz (RMS displacement: 3.1×10^{-4} µm) and 53 Hz (RMS displacement: 4.0×10^{-5} µm), which are the harmonics of 26.5 Hz. The information is listed in Table 1 for comparison with other vibration sources.

2.2.2. Polycold compact coolers (PCC) and turbomolecular pump (TMP). A rack containing two PCCs, shown in Fig. 2(*b*), is placed beside the TMP on the floor in the CMCF 08ID-1 experimental hutch. The PCCs and TMP are treated as one unit since they always work simultaneously. The accelerometer is mounted on the blue steel base, as shown in Fig. 1(*a*). Fig. 4 shows that PCCs and TMP induced vibrations with a frequency of 47.5 Hz (RMS displacement: 5.5×10^{-5} µm), 68 Hz (RMS displacement: 2.6×10^{-5} µm) and 76.5 Hz (RMS displacement: 1.3×10^{-5} µm). This information is also listed in Table 1. Table 1 shows that the fan coil unit causes larger vibration (in terms of RMS displacement) than the PCCs and TMP.

Table 1
Detailed information of identified vibration sources.

Frequency (Hz)	RMS displacement (µm)	Equipment	Beamlines/endstations
9.4	1.9×10^{-3} (z direction)	Detector cooling	HXMA 06ID-1 Micro-Probe endstation
12.2	1.5×10^{-3}	Cryostat system	SM 10ID-1 STXM
14.1	1.3×10^{-3}	Cryostat system	SM 10ID-1 STXM
14.6	6.4×10^{-3} (x direction)	Detector cooling	HXMA 06ID-1 Micro-Probe endstation
25.1	1.0×10^{-3} (x direction)	Detector cooling	HXMA 06ID-1 Micro-Probe endstation
25.5	2.0×10^{-4}	Fan coil unit	CMCF 08ID-1 SOE
26.5	3.1×10^{-4}	Fan coil unit	CMCF 08ID-1 SOE
27.2	2.9×10^{-4}	Chiller	HXMA 06ID-1 Optics Hutch
28.5	1.3×10^{-3} (y direction)	Detector cooling	HXMA 06ID-1 Micro-Probe endstation
29.7	1.5×10^{-3}	TriScroll pump	CMCF 08ID-1 SOE
32.0	2.3×10^{-3} (z direction)	Detector cooling	HXMA 06ID-1 Micro-Probe endstation
47.5	5.5×10^{-5}	PCCs and TMP	CMCF 08ID-1 SOE
53	4.0×10^{-5}	Fan coil unit	CMCF 08ID-1 SOE
59.4	1.2×10^{-4}	TriScroll pump	CMCF 08ID-1 SOE
68.0	2.6×10^{-5}	PCCs and TMP	CMCF 08ID-1 SOE
76.5	1.3×10^{-5}	PCCs and TMP	CMCF 08ID-1 SOE
89.1	4.7×10^{-5}	TriScroll pump	CMCF 08ID-1 SOE
Broad range: 20–80	–	Cryostat system	REIXS 10ID-2 endstation
Broad range: 40–120	–	Cryopump	REIXS 10ID-2 endstation
Broad range: 30–80	Details in Table 3	Cryostat system	SM 10ID-1 STXM

2.2.3. Vacuum pump. The Varian TriScroll pumps shown in Fig. 2(*c*) are widely used as rough vacuum pumps on many

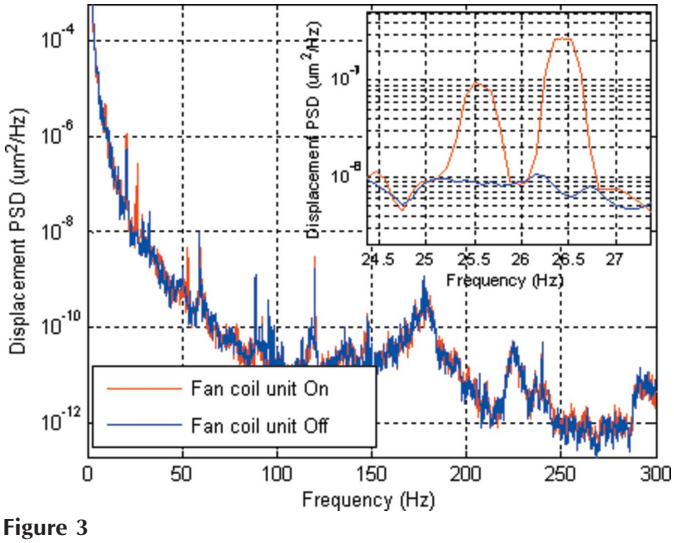

Figure 3
Floor vibrations when the fan coil unit is turned on/off.

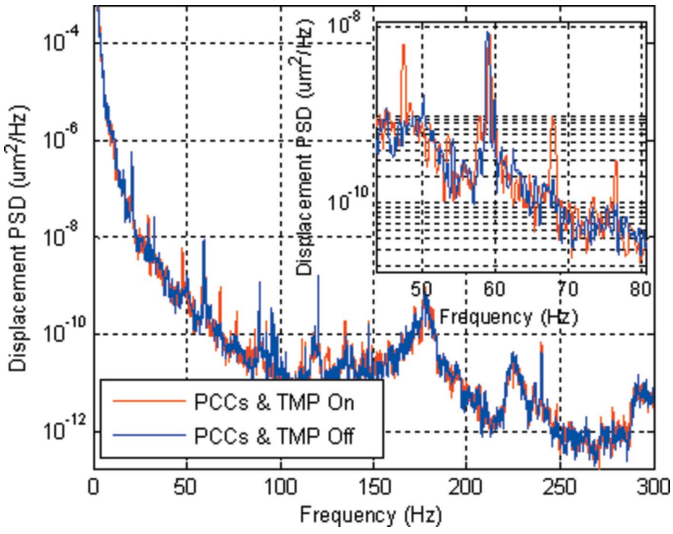

Figure 4
Floor vibrations when the PCCs and TMP are turned on/off.

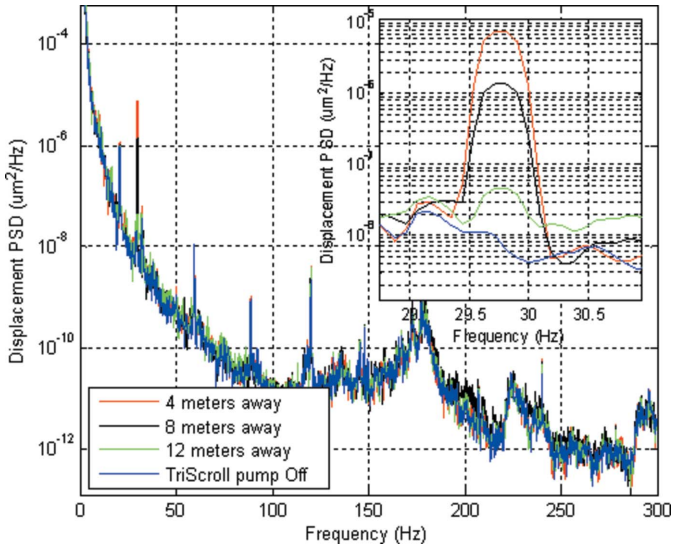

Figure 6
Distance effects on the Varian TriScroll pump-induced vibrations.

beamlines at the CLS. Fig. 5 shows the displacement PSD of the floor vibrations in the CMCF 08ID-1 SOE experimental hutch when the Varian TriScroll pump is turned on (red line) and off (blue line). Fig. 5 shows that the TriScroll pump induced vibrations with a frequency of 29.7 Hz (RMS displacement: 1.5×10^{-3} µm) and with harmonics of 59.4 Hz (RMS displacement: 1.2×10^{-4} µm) and 89.1 Hz (RMS displacement: 4.7×10^{-5} µm). This information is also listed in Table 1. Both Fig. 5 and Table 1 show that the Varian TriScroll pump produces the most significant vibrations (in terms of RMS displacement) on the CMCF 08ID-1 beamline [at the current development phase (March 2010)].

Since the Varian TriScroll pumps are widely used at the CLS and so far most of them are placed on the facility floor without using any carefully designed damping devices, it is necessary to investigate how far the facility floor needs to damp the pump-induced vibrations. Fig. 6 shows the displacement PSD of the floor vibrations when the Varian TriScroll pump is mounted at different locations on the floor, *i.e.* 4 m, 8 m and 12 m away from the accelerometer. The RMS displacements at different locations are 1.6×10^{-3} µm (4 m away), 7.2×10^{-4} µm (8 m away) and 1.7×10^{-4} µm (12 m away). Therefore, the facility floor needs at least 12 m to dampen Varian TriScroll pump-induced vibrations; in other words, any Varian TriScroll pumps located within 12 m might contribute to vibrations.

2.2.4. Chiller. The chiller shown in Fig. 2(*d*) is used for a water-cooling system and is approximately 3 m away from the monochromator outside the optics hutch at the HXMA 06ID-1 beamline. The monochromator is shown in Fig. 1(*c*). One accelerometer is mounted on top of the monochromator chamber shown in Fig. 1(*b*) and the other one is mounted on the floor under the monochromator platform shown in Fig. 1(*e*). Fig. 7 shows that when the chiller is turned on and the damping material is removed, both floor and mono-

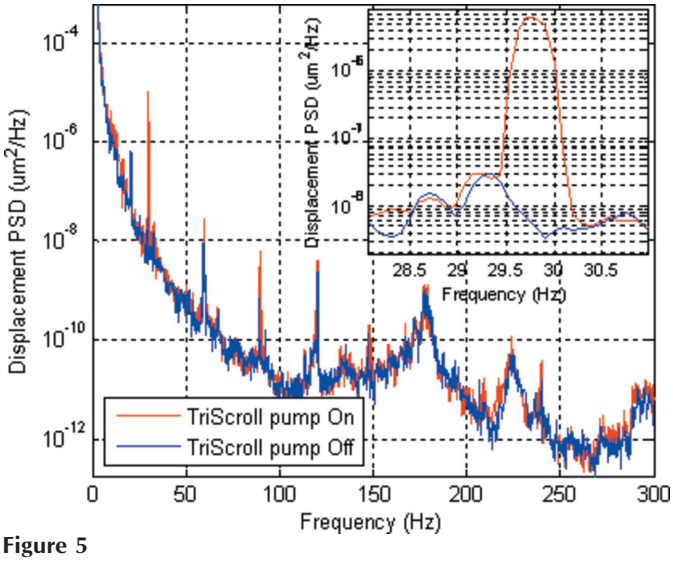

Figure 5
Floor vibrations when the Varian TriScroll pump in the SOE is turned on/off.

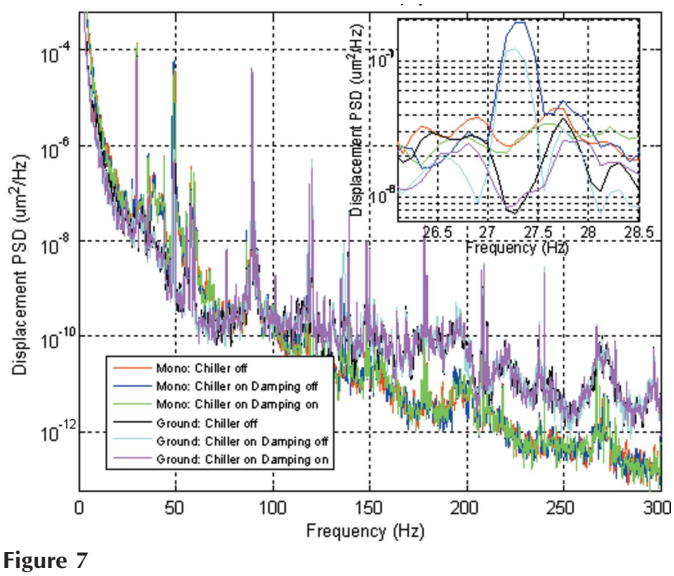

Figure 7
Vibration identification and isolation.

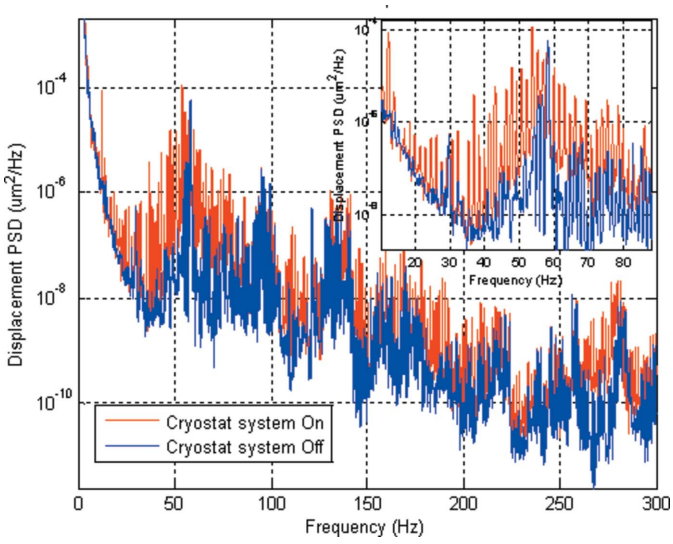

Figure 8
Cryostat system induced vibrations (in the vertical direction).

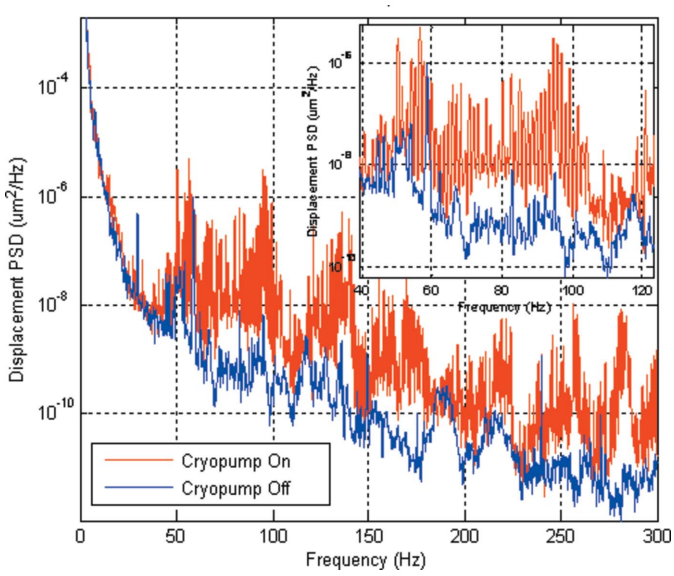

Figure 9
Cryopump-induced vibration (in the vertical direction).

chromator vibrations at a frequency of 27.2 Hz dramatically increase, compared with the vibrations when the chiller is turned off. This means that when the chiller is in normal operation it causes vibration with a frequency of 27.2 Hz and the vibration propagates from the floor to the monochromator. Fig. 7 also shows that, when the damping material is used, the vibration of 27.2 Hz disappeared from the monochromator and floor. This implies that the damping material used can effectively isolate the chiller-induced vibration.

2.2.5. Cryostat system. The cryostat compressor shown in Fig. 2(*e*) is placed outside of the REIXS 10ID-2 experimental hutch and is approximately 1.5 m away from the endstation which is shown in Fig. 1(*f*). Fig. 1(*f*) also shows two accelerometers are mounted on the blue steel frame supporting the endstation, in order to measure vibrations in the vertical direction and horizontal direction simultaneously. The cryostat system includes the cryostat compressor shown in Fig. 2(*e*) and a cold head inside the endstation chamber (not visible in the figure). The cold head and the cryostat compressor always work simultaneously and thus they are considered as one unit called the cryostat system here. Fig. 8 shows that the cryostat system produces vibrations with a very broad frequency range from approximately 20 Hz to 80 Hz and many of these vibrations have fairly large displacement PSDs (over 10^{-6} μm^2 Hz^{-1}). Similar observations were found in the horizontal direction, which are not shown in this paper.

The cryostat system does not as yet affect the REIXS 10ID-2 beamline owing to the relatively large beam spot (200 μm × 200 μm). However, it has been found that its operation significantly affects its neighbor SM 10ID-1 STXM endstation, which will be discussed later in §3.

2.2.6. Cryopump. The Helix Cryo Torr 8F cryopump compressor shown in Fig. 2(*f*) is located outside of the REIXS 10ID-2 experimental hutch and just beside the cryostat compressor. Fig. 9 shows that the cryopump produces vibrations with a very broad frequency range from approximately 40 Hz to 120 Hz, but most of these vibrations have relatively small displacement PSDs (below 10^{-6} μm^2 Hz^{-1}). Similar observations can be found from vibrations in the horizontal direction, not shown in this paper. So far no evidence has been found that the cryopump-induced vibrations cause problems for operations of either the REIXS 10ID-2 beamline or the STXM endstation.

2.2.7. Detector cooling system. The equipment as shown in Fig. 2(*g*) is used for cooling the detector of the MicroProbe endstation and it is approximately 0.5 m away from the microprobe endstation in the HXMA 06ID-1 experimental hutch. The microprobe endstation is very sensitive to vibrations since a very small beam spot (3 μm × 5 μm) is required. Thus, three-dimensional vibrations of the microprobe endstation were investigated; in particular, the effects of the detector cooling system on the endstation were studied. Since the VSA has only two channels, two accelerometers are mounted on the microprobe endstation in order to measure two-dimensional vibrations simultaneously, *e.g.* in the *y*–*z* direction as shown in Fig. 1(*h*). The accelerometers were then re-arranged to measure vibrations in the *x*–*z* direction (not shown in the figure).

Figs. 10, 11 and 12 show the displacement PSD of the microprobe endstation in the *x*, *y* and *z* direction, respectively. The RMS displacements and frequencies of vibrations with displacement PSD over 10^{-6} μm^2 Hz^{-1} are listed in Table 2. From Table 2 it can be seen that, when the detector cooling system is turned off, the total RMS displacements are 0.001 μm in the *x* direction, 0.0013 μm in the *y* direction and 0.0032 μm in the *z* direction. When the detector's cooling system is turned on, the total RMS displacements increase to 0.0130 μm in the *x* direction, 0.0054 μm in the *y* direction and 0.0109 μm in the *z* direction. This suggests that the operation of the detector's cooling system will significantly increase the vibration of the microprobe endstation by 1200% in the *x*

Table 2
Three-dimensional vibrations of the MicroProbe endstation.

Frequency (Hz)	*x* direction RMS (μm)		*y* direction RMS (μm)		*z* direction RMS (μm)	
	Turn on	Turn off	Turn on	Turn off	Turn on	Turn off
9.4	–	–	–	–	0.0019	–
14.6	0.0064	–	0.0030	–	0.0007	–
25.1	0.0010	–	–	–	–	–
28.1	–	0.0003	–	0.0006	–	0.0003
28.5	0.0011		0.0013	–	–	–
29.7	–	–	–	–	0.0005	0.0005
32.0	0.0021	–	–	–	0.0023	–
42.4	0.0009	–	–	–	–	–
42.7	–	–	0.0003	–	–	–
43.0	–	–	–	–	0.0031	–
48.3	0.0005	0.0005	0.0005	0.0005	0.0022	0.0022
55.4	0.0002	0.0002	0.0002	0.0002	0.0002	0.0002
67.5	0.0008	–	–	–	–	–
70.0	–	–	0.0001	–	–	–
Total RMS	0.0130	0.001	0.0054	0.0013	0.0109	0.0032

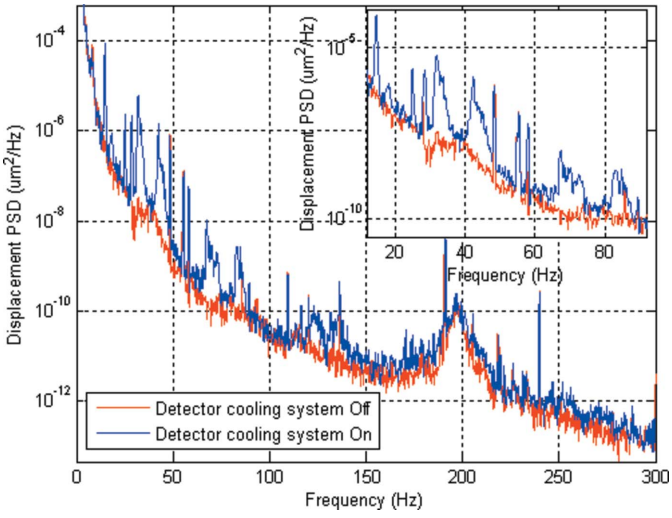

Figure 10
Vibration in the *x*-direction.

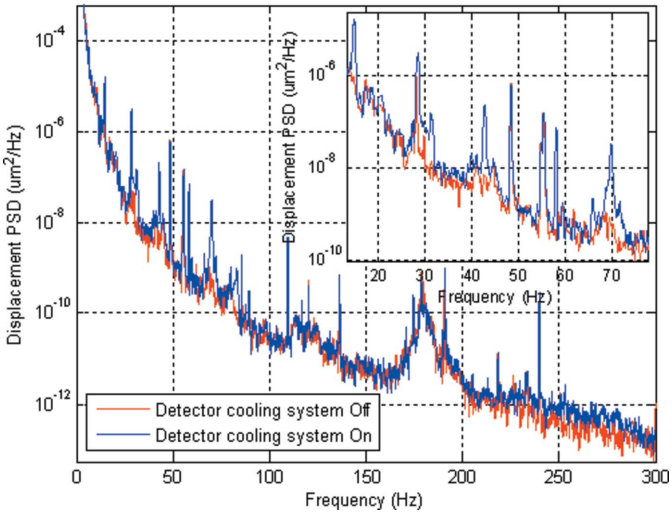

Figure 11
Vibrations in the *y*-direction.

direction, more than 300% in the *y* direction and approximately 240% in the *z* direction.

3. Effects of vibrations on the beamline

The cryostat system is a part of the REIXS 10ID-2 beamline but is very close (approximately 1.5 m) to the STXM endstation. The STXM endstation can produce images with spatial resolutions as fine as 30 nm. An example of an image obtained from the STXM endstation, of nitrogen-doped carbon nanotubes (N-CNT), is given in Fig. 13(*a*). This image was obtained when the cryostat system was not in operation and the profile of the N-CNT can be clearly observed. When the cryostat system was in full operation, however, the image of the N-CNT becomes quite disturbed as shown in Fig. 13(*b*). To investigate the effects of the cryostat-system-induced vibration on the STXM endstation, the accelerometer was mounted inside the endstation chamber to measure vibrations in the *y* and *z* directions, as shown in Fig. 1(*g*).

Figs. 14 and 15 show that the cryostat system produces vibrations with a broad frequency range of around 30 Hz to 80 Hz, which is consistent with the data collected in the REIXS 10ID-2 endstation (Fig. 8). Compared with the cryostat-system-induced vibrations in the REIXS 10ID-2 endstation (Fig. 8), some vibrations with low frequency (<30 Hz) caused by the cryostat system are almost completely damped by the STXM endstation platform, but the high-frequency vibrations (>30 Hz) are not significantly reduced, as shown in Fig. 15.

Vibrations with displacement PSD over 10^{-6} μm^2 Hz^{-1} are listed in Table 3. From this table it can be seen that, when the cryostat system is turned off, the total RMS displacements in

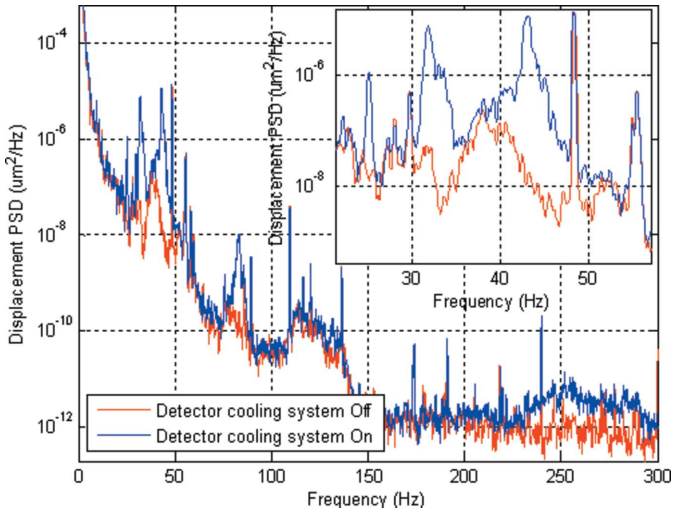

Figure 12
Vibrations in the *z*-direction.

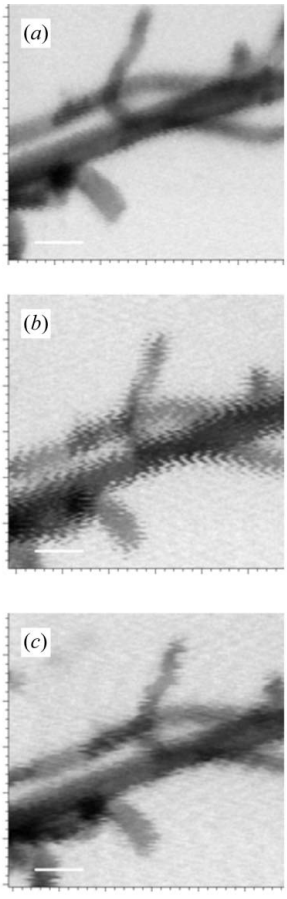

Figure 13
STXM images of N-CNT at 401.0 eV. Scale bar: 500 nm.

the y and z directions are 0.0214 µm and 0.0143 µm, respectively. It can be seen from the table that when the cryostat system is turned on the total RMS displacements in the y and z directions increase to 0.0265 and 0.0253 µm, respectively. This suggests that the operation of the cryostat system will increase

Table 3
Two-dimensional vibrations of the STXM endstation.

	y direction RMS (µm)		z direction RMS (µm)	
Frequency (Hz)	Turn on	Turn off	Turn on	Turn off
8.5	0.0147	0.0147	0.0032	0.0036
10.0	0.0033	0.0038	0.0028	0.0034
12.2	–	–	0.0015	–
14.1	–	–	0.0013	–
29.7	–	–	0.0026	0.0025
32.2	–	–	0.0015	–
38.3	0.0009	–	–	–
46.0	–	–	0.0009	–
47.6	–	–	0.0011	–
49.1	–	–	0.0012	–
52.1	–	–	0.0007	–
53.5	0.0027	–	0.0015	–
55.2	–	–	0.0007	–
56.6	0.0020	–	0.0006	–
58.2	0.0029	0.0029	0.0048	0.0048
59.8	–	–	0.0009	–
Total RMS	0.0265	0.0214	0.0253	0.0143

the vibration by almost 25% in the y direction and almost 80% in the z direction, which is likely to be responsible for the poor quality of the image shown in Fig. 13(b). To further confirm this, another image was taken at the STXM endstation when the vibration of the cryostat system was reduced by re-setting its parameters and the resulting image is shown in Fig. 13(c). It is clear that the quality of the image in Fig. 13(c) is in between Figs. 13(a) and 13(b). Therefore, it can be concluded that the cryostat system is one of the significant vibration sources affecting the performance of the STXM endstation. It can be further found from Table 3 that the vibrations with low frequencies (*e.g.* 8.5 Hz and 10.0 Hz) contribute approximately 50% of vibrations in terms of the RMS displacement. If the vibration sources with frequencies of 8.5 Hz and 10.0 Hz can be identified and isolated, it is expected that the quality of the images produced at the STXM endstation can be significantly improved.

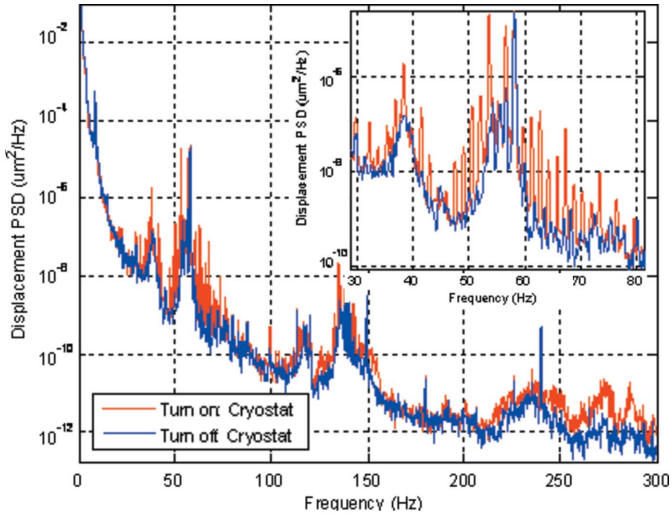

Figure 14
Vibrations in the y-direction on the STXM when the cryostat system is on/off.

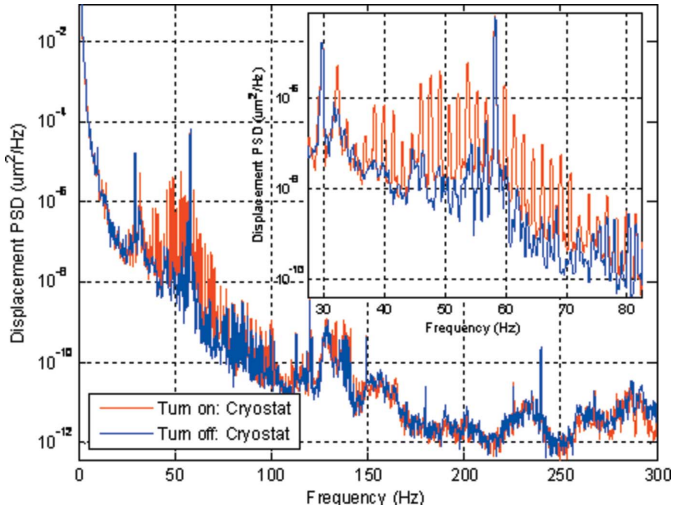

Figure 15
Vibrations in the z-direction on the STXM when the cryostat system is on/off.

4. Conclusions

In this paper seven vibration sources are identified at four beamlines/endstations at the CLS. The results demonstrate that movable mechanical equipment in the optics hutch and experimental hutch can cause vibrations significantly affecting the performance of these beamlines/endstations. The information provided in this paper is important for understanding and controlling vibrations not only for beamlines at the CLS but also for other synchrotron radiation facilities worldwide. In the future the influence of mechanical vibrations on the beamline will be investigated, and more vibration sources will be identified; designs for vibration suspension mechanisms will be developed at the CLS.

JWL would like to acknowledge financial support from the University of Saskatchewan and the Canadian Light Source Inc. through a graduate scholarship program. The work is also supported in part by the Natural Science and Engineering Research Council of Canada (NSERC) through a discovery grant. The authors thank Managing Editor Matthew Dalzell at the CLS for editing the manuscript.

References

Aleshaev, A. N., Fedotov, M. G., Gavrilov, N. G., Mishnev, S. I., Panchenko, V. E., Pindyurin, V. F., Poletaev, I. V. & Tolochko, B. P. (2001). *Nucl. Instrum. Methods Phys. Res. A*, **470**, 94–100.

Benmerrouche, M. & Hodges, A. (2010). CLSI Safety Report, Document No. 11.18.40.2. Canadian Light Source, Saskatoon, Saskatchewan, Canada.

Doose, C. & Sharma, S. (2002). *Proceedings of 2nd International Workshop on Mechanical Engineering Design of Synchrotron Radiation Equipment and Instrumentation*, 5–6 September 2002, Advanced Photon Source, Argonne National Laboratory, Argonne, Illinois, USA.

Fukuda, M., Endo, N., Tsuyuzaki, H., Suzuki, M. & Deguchi, K. (1996). *Jpn. J. Appl. Phys.* **35**, 6458–6462.

Huke, K. (1987). *Jpn. J. Appl. Phys.* **26**, 285–288.

Liu, Y. H., Wang, D. J., Chang, J. C. & Chen, J. R. (2007). *Proceedings of the 4th Asian Particle Accelerator Conference*, 29 January–2 February 2007, Raja Ramanna Centre for Advanced Technology, Indore, India, pp. 776–778.

Masuzawa, M., Sugahara, R. & Yamaoka, H. (2006). *Proceedings of the 9th International Workshop on Accelerator Alignment*, 26–29 September 2006, Stanford Linear Accelerator Center, Stanford, CA, USA.

Matsui, S., Oishi, M., Tanaka, H., Yorita, T., Tsumaki, K., Kumagai, N. & Nakazato, T. (2003). *Jpn. J. Appl. Phys.* **42**, L338–L341.

Michaelian, K. H., May, T. E. & Hyett, C. (2008). *Rev. Sci. Instrum.* **79**, 014903.

Nakazato, T., Date, S., Fukami, K., Matsui, S., Magome, T., Oishi, M., Soutome, K., Tanaka, H. & Yorita, T. (2002). *Proceedings of the 2nd International Workshop on Mechanical Engineering Design of Synchrotron Radiation Equipment and Instrumentation*, 5–6 September 2002, Advanced Photon Source, Argonne National Laboratory, Argonne, IL, USA.

Ouyang, L., Bu, L., Chen, J. & Wang, X. (2006). *International Workshop on Mechanical Engineering Design of Synchrotron Radiation Equipment and Instrumentation*, 24–26 May 2006, Egret Himeji, Hyogo, Japan.

Paulsen, J. (2006). *Vibration Data Acquisition System User's Manual*, Document No. 8.9.44.1. Canadian Light Source, Saskatoon, Saskatchewan, Canada.

Preissner, C. & Shu, D. (2006). *International Workshop on Mechanical Engineering Design of Synchrotron Radiation Equipment and Instrumentation*, 24–26 May 2006, Egret Himeji, Hyogo, Japan.

Tanaka, H. *et al.* (2002). *Proceedings of the 7th International Workshop on Accelerator Alignment*, 11–14 November 2002, Spring-8, Japan.

Terzano, R., Denecke, M. A. & Medici, L. (2010). *J. Synchrotron Rad.* **17**, 147–148.

Tsumaki, K. & Kumagai, N. (2001). *Proceedings of the 2001 Particle Accelerator Conference*, 18–22 June 2001, Chicago, IL, USA, pp. 1482–1484.

Wang, D. J., Perng, S. Y., Ho, H. C. & Kuan, C. K. (2002). *Proceedings of 2nd International Workshop on Mechanical Engineering Design of Synchrotron Radiation Equipment and Instrumentation*, 5–6 September 2002, Advanced Photon Source, Argonne National Laboratory, Argonne, IL, USA.

Wang, H. S., Wang, D. J., Perng, S. Y., Tseng, T. C., Lin, C. J., Ho, H. C. & Chen, J. R. (2006). *International Workshop on Mechanical Engineering Design of Synchrotron Radiation Equipment and Instrumentation*, 24–26 May 2006, Egret Himeji, Hyogo, Japan.

Wang, X., Chen, L., Du, H. & Yin, L. (2008*a*). *J. Synchrotron Rad.* **15**, 350–354.

Wang, X., Chen, L., Yan, Z., Du, H. & Yin, L. (2008*b*). *J. Synchrotron Rad.* **15**, 385–391.

Yates, B. W. & Hallin, E. L. (2002). *Rev. Sci. Instrum.* **73**, 1602–1604.

Yin, L. X., Du, H. W., Jiang, D. K., Zhou, Q. G., Yan, Z. B., Yu, C. H. & Wang, X. (2007). *Proceedings of the 4th Asian Particle Accelerator Conference*, 29 January–2 February 2007, Raja Ramanna Centre for Advanced Technology (RRCAT), Indore, India, pp. 755–757.